Moving target feature extraction with polarisation diversity in the presence of arbitrary range migration and phase errors

G.Liu, H.Li and J.Li

Abstract: High range resolution (HRR) moving target indication (MTI) is increasingly important in many military and civilian applications such as the detection and classification of moving targets in strong clutter backgrounds. Meanwhile using polarisation diversity in radar systems has been shown to result in improved performance as compared with using only a single polarisation channel. The authors extract HRR moving target features with polarisation diversity in the presence of strong stationary clutter. The problem considered takes into account arbitrary range migration and phase errors, which may be induced by unknown target and platform motions as well as atmosphere turbulence and/or system instability. A relaxation-based algorithm is presented for the joint clutter suppression and super resolution target feature extraction and its performance is compared to the Cramér–Rao bound, the best performance bound an unbiased estimator can achieve. Numerical results are also provided to demonstrate the performance of the proposed algorithm.

1 Introduction

Moving target feature extraction has long been a widely investigated topic in the literature because of its extensive applications in both military and civilian areas, such as automatic target recognition (ATR) of non-cooperative targets [1, 2], surveillance of battle fields [3], and ground traffic control at airports [4]. A conventional moving target indication (MTI) radar [5] is designed with low resolution primarily for detecting, locating and tracking moving targets in a clutter environment.

Both inverse synthetic aperture radars (ISARs) and high range resolution (HRR) radars [6] have been used to extract moving target features. The former can provide high resolution features of moving targets in both range and cross-range by using sophisticated algorithms to compensate for the non-cooperative motion between the radar sensor and the targets, whereas the latter is able to produce high resolution features only in range but requires relatively simple signal processing algorithms and much shorter dwell time. Special attention has recently been paid to the combination of the HRR and MTI for moving target feature extraction [7].

An HRR MTI radar can not only add the ATR function to the conventional MTI radar, but also enhance its capability of detecting, locating and tracking moving targets since the signal-to-clutter ratio (SCR) can be increased by reducing the size of the clutter cell. Three important technical issues associated with the signal processing of HRR MTI radars include clutter suppression, motion compensation, and feature extraction. Unlike a conventional low-resolution MTI radar that uses a pulse canceller to suppress the stationary clutter to indicate the moving targets, an HRR MTI radar is expected to provide high resolution range features of even slowly moving targets in the clutter. If the clutter is not suppressed effectively, the target range signatures will be of little use in practical applications. As for the motion compensation, the range migration resulted from the radial motion between the radar and the target will accumulate from pulse to pulse and destroy the range alignment. The quality of the HRR range signature, which is a key factor to the success of ATR, can also be degraded drastically by the inappropriately compensated phase errors due to unknown target and platform motions as well as atmosphere turbulence and/or system instability. Since the conventional matched filtering approach cannot resolve two signals with a time spacing less than the reciprocal of the signal bandwidth, super resolution approaches are needed to obtain better feature extraction performances.

Polarisation diversity [8, 9] has been an important technique for improved application performances. In a full-polarisation radar configuration, the diversity is exploited in both transmission and reception, which enables the radar to measure the complete complex scattering matrix for each resolution cell in a scene. The availability of the scattering matrix makes it possible to calculate the radar response of a scatterer for any possible polarisation combination of transmitting and receiving antennas by means of polarisation synthesis. A large number of approaches have been proposed in literature [10–12], to use polarisation diversity for improved performance of target detection, ATR, and distributed target discrimination.

IEE Proceedings online no. 20000464

DOI: 10.1049/ip-rsn:20000464

Paper first received 8th November 1999 and in revised form 14th March 2000

G. Liu and J. Li are with the Department of Electrical and Computer Engineering, University of Florida, Gainesville, FL 32611, USA

H. Li is with the Department of Electrical and Computer Engineering, Stevens Institute of Technology, Hoboken, NJ 07030, USA

We study the feature extraction of moving targets with closely spaced scatterers in the presence of strong stationary clutter for HRR MTI radars with polarisation diversity. For each individual polarisation channel, the received signal after dechirping consists of multiple complex sinusoids, the clutter, and the noise. The sinusoidal model is characterised by the frequencies proportional to the locations of the scatterers in range, the complex scattering matrix whose elements are the amplitudes corresponding to the radar cross-sections (RCSs) measured in each polarisation channel, the range migration of each scatterer, and the phase errors. In practice, due to the manoeuvres of the target and the unknown platform motion, the range migration may be arbitrary, and so are the phase errors because of such range migration, and/or atmospheric turbulences, and/or system instability. Unlike [7] that does not take into account the range migration, our model considers both the arbitrary range migration and arbitrary phase errors. In addition, the clutter is assumed to be polarisation-dependent but stationary during the short dwell time, and the noise is assumed to be a zero-mean complex white gaussian random process.

A relaxation-based algorithm is proposed to extract the polarimetric HRR features of a moving target with arbitrary pulse-to-pulse range migration and arbitrary phase errors in the presence of strong stationary clutter. The proposed algorithm consists of three steps, namely, clutter suppression, motion parameter (range migration and phase error) estimation, and feature (range and amplitude) extraction. The feature estimates are obtained by minimising a nonlinear least squares (NLS) cost function via a series of one-dimensional (1-D) fast Fourier transforms (FFTs). Particularly, MODE (method of direction estimation) [13–15] and MRELAX (multi-snapshot RELAX) [16] are jointly used in the feature extraction step. The algorithm is computationally simple and converges quickly for targets consisting of closely spaced scatterers.

2 Data model and problem formulation

We first establish the data model for single-polarisation HRR MTI radars and then extend the model into the multi-polarisation case.

2.1 Single-polarisation case

The range resolution of a radar is determined by the transmitted signal bandwidth. To achieve high range resolution, a radar must transmit wideband pulses, which are often linear frequency modulated (LFM) signals. For a single-polarisation configuration, assume that the pulse width is T_0 and the pulse repetition interval (PRI) is T. Then a normalised chirp signal has the form

$$s(t) = e^{j(2\pi f_0 t + \gamma t^2)}, \quad |t| \le T_0/2 \tag{1}$$

where f_0 denotes the carrier frequency and 2γ denotes the chirp rate. We assume that the target of interest has K scatterers with different radial velocities. Let L be the total number of pulses transmitted in a coherent processing interval (CPI). Then when the lth pulse is transmitted, the range of the kth scatterer is $R_k(l) = R_k + \Delta R_k(l)$, $k = 1, \ldots, K$, where R_k denotes the range location of the kth scatterer when the first pulse is transmitted, and $\Delta R_k(l)$ the range migration of the kth scatterer during the first l pulse intervals. Obviously, $\Delta R_k(0) = 0$. Let $\tilde{t} = t - lT$ denote the *fast time*, the received signal from the kth scatterer corresponding to the lth transmitted pulse is

$$r_k(\tilde{t}, l) = \tilde{\alpha}_k \exp\left\{ j\left[2\pi f_0 \left(\tilde{t} - \tau_0 - \Delta\tau_k - \frac{2\Delta R_k(l)}{c} \right) + \gamma \left(\tilde{t} - \tau_0 - \Delta\tau_k - \frac{2\Delta R_k(l)}{c} \right)^2 \right] \right\} \tag{2}$$

where $\tilde{\alpha}_k$ is determined by the RCS of the kth scatterer, $\tau_0 = 2R_0/c$, and $\Delta\tau_k = 2(R_k - R_0)/c$, with R_0 denoting a reference range (possibly corresponding to the target centre) and c the speed of light. By using $s(\tilde{t} - \tau_0)$ as the reference signal the dechirped signal has the form

$$\begin{aligned} d_k(\tilde{t}, l) &= r_k(\tilde{t}, l) s^*(\tilde{t} - \tau_0) \\ &= \tilde{\alpha}_k \exp\left[-j2(\pi f_0 + \gamma\tilde{t} - \gamma\tau_0)\left(\Delta\tau_k + \frac{2\Delta R_k(l)}{c} \right) \right] \\ &\quad \exp\left[j\gamma \left(\Delta\tau_k + \frac{2\Delta R_k(l)}{c} \right)^2 \right] \end{aligned} \tag{3}$$

where the $(\cdot)^*$ means the complex conjugate. Since both $\Delta R_k(l)/c$ and $\Delta\tau_k$ tend to be very small in practical when the dwell time is short, we can approximately express eqn. 3 as

$$\begin{aligned} d_k(\tilde{t}, l) &\simeq \tilde{\alpha}_k \exp[-j2(\pi f_0 - \gamma\tau_0)\Delta\tau_k] \exp[-j2\gamma\Delta\tau_k\tilde{t}] \\ &\quad \exp\left[-j\frac{4\gamma\Delta R_k(l)}{c}\tilde{t} \right] \exp\left[-j\left(\frac{4\pi}{\lambda} - \frac{4\gamma\tau_0}{c} \right)\Delta R_k(l) \right] \end{aligned} \tag{4}$$

where λ denotes the radar operation wavelength. Note that in eqn. 4, the first exponential term is a constant and may be absorbed into $\tilde{\alpha}_k$; the phase of the second term is a linear function of $\tilde{t}$, which describes the phase history of the kth scatterer within the lth chirp pulse; the third term represents the accumulated phase shift from pulse to pulse, which is the range migration; the last term accounts for the phase shift related to the radial motion of the kth scatterer.

We assume that $2(R_{max} - R_{min})/c \ll T_0$, where R_{max} and R_{min} denote the maximum and minimum ranges between the radar and target scatterers, respectively. Let T_s denote the sampling period. Then we can express the sampled dechirped signal as

$$\tilde{d}(n, l) = \left(\sum_{k=0}^{K} \alpha_k e^{j2\pi f_k n} \right) e^{j2\pi\bar{f}_{kl} n} e^{j\psi_{kl}},$$
$$n = 0, \cdots, N-1, \quad l = 0, \cdots, L-1 \tag{5}$$

where

$$\alpha_k = \tilde{\alpha}_k \exp[-j2(\pi f_0 - \gamma\tau_0)\Delta\tau_k] \tag{6}$$

$$f_k = -\frac{\gamma\Delta\tau_k T_s}{\pi} \tag{7}$$

$$\bar{f}_{kl} = -\frac{2\gamma\Delta R_k(l) T_s}{\pi c} \tag{8}$$

and

$$\psi_{kl} = \left(\frac{4\gamma\tau_0}{c} - \frac{4\pi}{\lambda} \right)\Delta R_k(l) \tag{9}$$

The phase shift ψ_{kl} is proportional to the range migration $\Delta R_k(l)$, and the ratio of $\bar{f}_{kl}$ to ψ_{kl} is a constant. This relationship may be used to simplify the model as well as the parameter estimation. However, this relationship may

not hold in practice since the phase error may be used to include other unknown factors besides the range migration, such as the wave propagation fluctuation and the system instability, which were not accounted for in the derivation. Therefore we assume herein the phase errors to be arbitrary to include all possible phase error sources.

Since most man-made radar targets have rigid bodies we assume that all scatterers of a target have the same amount of range migration and phase errors. Concerning the clutter measurement by an HRR radar, the clutter in nature is usually stationary and fluctuates little during a short dwell time. Although the multiplicative speckle model which arises under the assumption that many small scatterers, without a dominant one, are randomly distributed in each resolution cell is likely to apply in natural clutter environment, it is not necessarily an adequate model for a scenario where the speckle is not fully developed owing to the presence of hard moving targets and/or strong stable clutter varying in space. In addition, we assume that the radar illuminates a small azimuth range in the broadside direction and no internal clutter motion occurs so that the clutter Doppler can be ignored. Therefore we model the clutter as an arbitrary deterministic unknown sequence in range but fixed from pulse to pulse during the short dwell time. Then the dechirped signal in the presence of clutter and noise can be expressed as

$$y(n,l)=\left(\sum_{k=1}^{K}\alpha_k e^{j2\pi f_k n}\right)e^{j2\pi\bar{f}_l n}e^{j\psi_l}+c(n)+e(n,l)$$
$$n=0,1,\cdots,N-1,\quad l=0,1,\cdots,L-1 \tag{10}$$

where $c(n)$ and $e(n, l)$, respectively, denote the 1-D unknown clutter and 2-D random noise.

2.2 Multipolarisation case

Polarisation diversity enables a radar to measure complete complex scattering matrix for each target scatterer. When two orthogonally polarised antennas, usually horizontally polarised (H-polarised) and vertically polarised (V-polarised), are used jointly for transmission and reception, a total of four elements α_{HH}, α_{HV}, α_{VH} and α_{VV}, can be obtained for a scatterer. Here, for instance, HV stands for the H-polarised return given that the transmitted wave is V-polarised. The reciprocity theorem [17] states that $\alpha_{HV}=\alpha_{VH}$ for the backscattering case. Consequently, three independent elements of the polarimetric measurements form the scattering matrix of a scatterer, i.e.

$$\boldsymbol{S}=\begin{bmatrix}\alpha_{HH} & \alpha_{HV}\\ \alpha_{HV} & \alpha_{VV}\end{bmatrix} \tag{11}$$

With this preparation, we can build a polarimetric data model for moving target feature extraction by replacing the amplitude parameters in eqn. 10 with the corresponding elements in the scattering matrix of the scatterer. Let $j=1,\ldots,J$, with J being the total number of channels ($J=3$ in the case under discussion), denote the HH, HV and VV polarisation channels. We have the following expression for the phase history data model for the jth channel:

$$y_j(n,l)=\left(\sum_{k=1}^{K}\alpha_{kj}e^{j2\pi f_k n}\right)e^{j2\pi\bar{f}_{lj}n}e^{j\psi_{lj}}+c_j(n)+e_j(n,l)$$
$$n=0,1,\cdots,N-1,\quad l=0,1,\cdots,L-1,\quad j=1,\cdots,J \tag{12}$$

where α_{kj}, $j=1, 2, 3$, denote, respectively, the elements α_{HH}, α_{VH}, and α_{VV}, in the scattering matrix of the kth scatterer, $\bar{f}_{lj}$ and ψ_{lj} represent, respectively, the range migration and phase error in the lth pulse for the jth polarisation channel, and $c_j(n)$ and $e_j(n, l)$ are the 1-D stationary clutter and the 2-D random noise in the jth polarisation channel, respectively. There are two cases of interest for full-polarisation radar configuration.

Case 1: The time difference between transmitting the H- and V-polarised signals is very small with respect to the PRI. The range migration and phase errors vary very little during this small time interval. Then eqn. 12 holds with $J=3$, and $\bar{f}_{lj}=\bar{f}_l$, $\psi_{lj}=\psi_l$, for $j=1, 2, 3$, and $l=0,\ldots, L-1$. In this case, the phase history data model reduces to

$$y_j(n,l)=\left(\sum_{k=1}^{K}\alpha_{kj}e^{j2\pi f_k n}\right)e^{j2\pi\bar{f}_l n}e^{j\psi_l}+c_j(n)+e_j(n,l)$$
$$n=0,1,\cdots,N-1;\quad l=0,1,\cdots,L-1;\quad j=1,\cdots,J \tag{13}$$

To avoid model ambiguities we use the first pulse ($l=0$) as the reference and set $\bar{f}_0=0$ and $\psi_0=0$.

Case 2: Each H- and V-polarised transmitted pulse is offset in time from one another by a half PRI. The VV (or HH) signal will introduce a difference set of motion parameters compared to those contained in the other two channels. Then the polarimetric feature extraction problem becomes more complicated since a dual-polarisation case (e.g. HH–HV) corresponding to $J=2$ in eqn. 13 and a single-polarisation case (VV) corresponding to eqn. 10, or $J=1$ in eqn. 13, need to be considered separately for motion parameter estimation and motion compensation. In this case, for the HH–HV configuration, $\bar{f}_{lj}=\bar{f}_l$, $\psi_{lj}=\psi_l$, for $j=1$, 2 and $l=0,\ldots, L-1$. Further, $\bar{f}_{01}=\bar{f}_{02}=0$ and $\psi_{01}=\psi_{02}=0$ are assumed. For the VV channel, a real-valued amplitude is assumed to avoid phase ambiguity. This assumption is valid for the basic reflection modes such as reflections from large conducting spheres, dihedral and trihedral corner reflectors [8].

For the simplicity, we discuss primarily case 1. The solution corresponding to case 2 can be similarly obtained by making some simple modifications. Let

$$\boldsymbol{y}_j=\begin{bmatrix}\boldsymbol{y}_{0j}^T & \boldsymbol{y}_{1j}^T & \cdots & \boldsymbol{y}_{L-1j}^T\end{bmatrix}^T\in C^{LN\times 1},\quad j=1,\cdots,J \tag{14}$$

where $(\cdot)^T$ denotes the transpose, and

$$\boldsymbol{y}_{lj}=\begin{bmatrix}y_j(0,l) & y_j(1,l) & \cdots & y_j(N-1,l)\end{bmatrix}^T,\quad l=0,1,\cdots,L-1,\quad j=1,\cdots,J \tag{15}$$

Then eqn. 13 can be rewritten in a vector form as

$$\boldsymbol{y}_j=\bar{\boldsymbol{f}}\odot\left[(\boldsymbol{\psi}\otimes\boldsymbol{A})\boldsymbol{a}_j\right]+\boldsymbol{u}_L\otimes\boldsymbol{c}_j+\boldsymbol{e}_j,\quad j=1,\cdots,J \tag{16}$$

where $\odot$ and $\otimes$ denote, respectively, the Hadamard and Kronecker matrix products of two matrices [18], $\boldsymbol{e}_j$ is an $(NL)\times 1$ vector formed from $\{e_j(n, l)\}$ in the same way as $\boldsymbol{y}_j$ from $\{y_j(n, l)\}$

$$\boldsymbol{u}_L=\begin{bmatrix}1 & 1 & \cdots & 1\end{bmatrix}^T\in R^{L\times 1} \tag{17}$$

$$\boldsymbol{c}_j=\begin{bmatrix}c_j(0) & c_j(1) & \cdots & c_j(N-1)\end{bmatrix}^T \tag{18}$$

$$\bar{\boldsymbol{f}}=\begin{bmatrix}\bar{\boldsymbol{f}}_0^T & \bar{\boldsymbol{f}}_1^T & \cdots & \bar{\boldsymbol{f}}_{L-1}^T\end{bmatrix}^T \tag{19}$$

with

$$\bar{\boldsymbol{f}}_l = \begin{bmatrix} 1 & e^{2\pi\bar{f}_l} & \cdots & e^{j2\pi\bar{f}_l(N-1)} \end{bmatrix}^T, \quad l = 0, \cdots, L-1 \tag{20}$$

$$\boldsymbol{\psi} = \begin{bmatrix} e^{j\psi_0} & e^{j\psi_1} & \cdots & e^{j\psi_{L-1}} \end{bmatrix}^T \tag{21}$$

$$\boldsymbol{a}_j = \begin{bmatrix} \alpha_{1j} & \alpha_{2j} & \cdots & \alpha_{Kj} \end{bmatrix}^T, \quad j = 1, \cdots, J \tag{22}$$

and

$$\boldsymbol{A} = \begin{bmatrix} \boldsymbol{a}_1 & \boldsymbol{a}_2 & \cdots & \boldsymbol{a}_K \end{bmatrix} \tag{23}$$

with

$$\boldsymbol{a}_k = \begin{bmatrix} 1 & e^{j2\pi f_k} & \cdots & e^{j2\pi f_k(N-1)} \end{bmatrix}^T, \quad k = 1, \cdots, K \tag{24}$$

The problem of interest is to suppress the clutter, to estimate the range migrations and phase errors, $\{\bar{f}_l, \psi_l\}_{l=0}^{L-1}$, for motion compensation, and to extract the target features, $\{\{\alpha_{kj}\}_{j=1}^J, f_k\}_{k=1}^K$, from the phase history data acquired by the polarimetric HRR MTI radar.

3 Relaxation-based algorithm for parameter estimation

The nonlinear least squares (NLS) estimates $\{\{\{\hat{\alpha}_{kj}\}_{j=1}^J, \hat{f}_k\}_{k=1}^K, \{\hat{\bar{f}}_l, \hat{\psi}_l\}_{l=1}^{L-1}, \{\hat{\boldsymbol{c}}_j\}_{j=1}^J\}$ of $\{\{\{\alpha_{kj}\}_{j=1}^J, f_k\}_{k=1}^K, \{\bar{f}_l, \psi_l\}_{l=1}^{L-1}, \{\boldsymbol{c}_j\}_{j=1}^J\}$ can be obtained by minimising the following NLS criterion

$$C_1\left(\{\{\alpha_{kj}\}_{j=1}^J, f_k\}_{k=1}^K, \{f_l, \psi_l\}_{l=1}^{L-1}, \{\boldsymbol{c}_j\}_{j=1}^J\right) = \sum_{j=1}^{J} \|\boldsymbol{y}_j - \bar{\boldsymbol{f}} \odot [(\boldsymbol{\psi} \otimes \boldsymbol{A})\boldsymbol{a}_j] - \boldsymbol{u}_L \otimes \boldsymbol{c}_j\|^2 \tag{25}$$

where $\|\cdot\|$ denotes the Euclidean norm. The minimisation of the cost function C_1 in eqn. 25 is a complicated nonlinear optimisation problem. A alternating optimisation algorithm is presented below for joint clutter suppression and parameter estimation, which is guaranteed to converge to at least a local optimum under mild conditions [19].

3.1 Clutter suppression

The stationary clutter can be suppressed by subtracting the estimated clutter $\{\hat{\boldsymbol{c}}_j\}_{j=1}^J$ from the measured data $\boldsymbol{y}_j$, $j = 1, \ldots, J$. Assume that the estimates $\{\{\hat{\alpha}_{kj}\}_{j=1}^J, \hat{f}_k\}_{k=1}^K$ and $\{\hat{\bar{f}}_l, \hat{\psi}_l\}_{l=1}^{L-1}$ are given and used in eqn. 25 to replace $\{\{\alpha_{kj}\}_{j=1}^J, f_k\}_{k=1}^K$ and $\{\bar{f}_l, \psi_l\}_{l=1}^{L-1}$, respectively. Then minimising C_1 in eqn. 25 with respect to $\{\boldsymbol{c}_j\}_{j=1}^J$ becomes minimising the following least squares criterion:

$$C_2(\{\boldsymbol{c}_j\}_{j=1}^J) = \sum_{j=1}^{J} \|\check{\boldsymbol{y}}_j - \boldsymbol{u}_L \otimes \boldsymbol{c}_j\|^2 \tag{26}$$

where

$$\check{\boldsymbol{y}}_j = \boldsymbol{y}_j - \hat{\bar{\boldsymbol{f}}} \odot \left[(\hat{\boldsymbol{\psi}} \otimes \hat{\boldsymbol{A}}\hat{\boldsymbol{a}}_j\right] \triangleq \begin{bmatrix} \check{\boldsymbol{y}}_{0j}^T & \check{\boldsymbol{y}}_{1j}^T & \cdots & \check{\boldsymbol{y}}_{L-1j}^T \end{bmatrix}^T, \quad j = 1, \cdots, J \tag{27}$$

A straightforward calculation gives

$$\hat{\boldsymbol{c}}_j = \frac{1}{L}\sum_{l=0}^{L-1} \check{\boldsymbol{y}}_{lj}, \quad j = 1, \cdots, J \tag{28}$$

which is the average of $\check{\boldsymbol{y}}_{lj}$, $l = 0, \ldots, L-1$, obtained by removing the estimated target signal from the received signal $\boldsymbol{y}_j$ in the jth polarisation channel.

3.2 Moving target feature estimation

Assume that the clutter estimate $\{\hat{\boldsymbol{c}}_j\}_{j=1}^J$ is available. Then the NLS estimates of $\{\{\alpha_{kj}\}_{j=1}^J, f_k\}_{k=1}^K$ and $\{\bar{f}_l, \psi_l\}_{l=1}^{L-1}$ can be obtained by minimising the following cost function:

$$C_3\left(\{\{\alpha_{kj}\}_{j=1}^J, f_k\}_{k=1}^K, \{\bar{f}_l, \psi_l\}_{l=1}^{L-1}\right) = \sum_{j=1}^{J} \|\check{\boldsymbol{y}}_j - \bar{\boldsymbol{f}} \odot \left[(\boldsymbol{\psi} \otimes \boldsymbol{A})\boldsymbol{a}_j\right]\|^2 \tag{29}$$

where

$$\check{\boldsymbol{y}}_j = \boldsymbol{y}_j - \boldsymbol{u}_L \otimes \hat{\boldsymbol{c}}_j \triangleq \begin{bmatrix} \check{\boldsymbol{y}}_{0j}^T & \check{\boldsymbol{y}}_{1j}^T & \cdots & \check{\boldsymbol{y}}_{L-1j}^T \end{bmatrix}^T, \quad j = 1, \cdots, J \tag{30}$$

The estimates $\{\{\hat{\alpha}_{kj}\}_{j=1}^J, \hat{f}_k\}_{k=1}^K$ and $\{\hat{\bar{f}}_l, \hat{\psi}_l\}_{l=1}^{L-1}$ of $\{\{\alpha_{kj}\}_{j=1}^J, f_k\}_{k=1}^K$ and $\{\bar{f}_l, \psi_l\}_{l=1}^{L-1}$, respectively, can be determined by minimising C_3 in eqn. 29 via an alternating optimisation approach, i.e. by letting only the parameters $\{\{\alpha_{kj}\}_{j=1}^J, f_k\}_{k=1}^K$ vary and fixing $\{\hat{\bar{f}}_l, \hat{\psi}_l\}_{l=1}^{L-1}$ at their most recently determined values and *vice versa*.

3.2.1 Motion estimation: When the feature estimates $\{\{\hat{\alpha}_{kj}\}_{j=1}^J, \hat{f}_k\}_{k=1}^K$ are given, minimising C_3 becomes minimising

$$C_4\left(\{\bar{f}_l, \psi_l\}_{l=1}^{L-1}\right) = \sum_{j=1}^{J} \left\|\check{\boldsymbol{y}}_j - \bar{\boldsymbol{f}} \odot \left[(\boldsymbol{\psi} \otimes \hat{\boldsymbol{A}})\hat{\boldsymbol{a}}_j\right]\right\|^2 \tag{31}$$

or, equivalently,

$$C_5(\bar{f}_l, \psi_l) = \sum_{j=1}^{J} \left\|\check{\boldsymbol{y}}_{lj} - \left[\bar{\boldsymbol{f}}_l \odot \left(\hat{\boldsymbol{A}}\hat{\boldsymbol{a}}_j\right)\right]e^{j\psi_l}\right\|^2, \quad l = 1, \cdots, L-1 \tag{32}$$

Minimising eqn. 32 yields

$$\hat{\bar{f}}_l = \arg\max_{\bar{f}_l} |\bar{\boldsymbol{f}}_l^H \bar{\boldsymbol{y}}_l|, \quad l = 1, \cdots, L-1 \tag{33}$$

and

$$\hat{\psi}_l = \text{angle}\left(\hat{\bar{\boldsymbol{f}}}_l^H \bar{\boldsymbol{y}}_l\right), \quad l = 1, \cdots, L-1 \tag{34}$$

where

$$\bar{\boldsymbol{y}}_l = \frac{1}{J}\sum_{j=1}^{J}\left[\check{\boldsymbol{y}}_{lj} \odot (\hat{\boldsymbol{A}}\hat{\boldsymbol{a}}_j)^*\right] \tag{35}$$

$\hat{\bar{\boldsymbol{f}}}_l$ is the same as $\bar{\boldsymbol{f}}_l$ except that $\bar{f}_l$ is replaced by $\hat{\bar{f}}_l$, $(\cdot)^H$ denotes the conjugate transpose, and angle (x) is the phase of x. Note that $\hat{\bar{f}}_l$ can be obtained by using 1-D FFT with zero-paddings to set an initial estimate, which can be refined then by using the FMIN function of MATLAB.

3.2.2 Feature extraction: Once the motion estimates $\{\hat{\bar{f}}_l, \hat{\psi}_l\}_{l=1}^{L-1}$ are available, the NLS estimates of $\{\{\alpha_{kj}\}_{j=1}^J, f_k\}_{k=1}^K$ can be obtained by minimising the following cost function:

$$C_6\left(\{\{\alpha_{kj}\}_{j=1}^J, f_k\}_{k=1}^K\right) = \sum_{j=1}^{J} \left\|\check{\boldsymbol{y}}_j - \hat{\bar{\boldsymbol{f}}} \odot \left[(\hat{\boldsymbol{\psi}} \otimes \boldsymbol{A})\boldsymbol{a}_j\right]\right\|^2 \tag{36}$$

or, equivalently,

$$C_7\left(\{\{\alpha_{kj}\}_{j=1}^{J}, f_k\}_{k=1}^{K}\right) = \sum_{j=1}^{J} \|\tilde{\boldsymbol{y}}_j - \boldsymbol{A}\boldsymbol{a}_j\|^2 \quad (37)$$

where

$$\tilde{\boldsymbol{y}}_j = \frac{1}{L}\sum_{l=0}^{L-1}\left[\check{\boldsymbol{y}}_{lj} \odot \left(\hat{\bar{\boldsymbol{f}}}_l^{*} e^{-j2\pi\hat{\psi}_l}\right)\right], j = 1, \cdots, J \quad (38)$$

Note that eqn. 38 can be interpreted as the temporal average of clutter suppressed and motion compensated polarimetric measurements. The multisnapshot RELAX (MRELAX) algorithm [16] can be employed to obtain the feature estimates $\{\{\hat{\alpha}_{kj}\}_{j=1}^{J}, \hat{f}_k\}_{k=1}^{K}$ of $\{\{\alpha_{kj}\}_{j=1}^{J}, f_k\}_{k=1}^{K}$.

When the target scatterers are closely spaced in range, i.e. some of the range frequencies $\{f_k\}_{k=1}^{K}$ are within one half of $1/N$ or less, the MRELAX algorithm tends to converge slowly and the accuracy of $\{\{\hat{\alpha}_{kj}\}_{j=1}^{J}, \hat{f}_k\}_{k=1}^{K}$ is poor, although the estimates $\{\hat{\bar{f}}_l, \hat{\psi}_l\}_{l=1}^{L-1}$ and $\{\hat{\boldsymbol{c}}_j\}_{j=1}^{J}$ may still be satisfying. To improve the accuracy of $\{\{\hat{\alpha}_{kj}\}_{j=1}^{J}, \hat{f}_k\}_{k=1}^{K}$ in this case, we utilise a modified version of the MODE algorithm [13–15].

The MODE estimates of the frequencies are asymptotically statistically efficient [13–15]. Once the MODE range frequency estimates $\{\hat{f}_k\}_{k=1}^{K}$ are obtained from the $\tilde{\boldsymbol{y}}_j$, $j = 1, \ldots, J$, in eqn. 38, the least squares estimates of $\{\{\alpha_{kj}\}_{j=1}^{J}\}_{k=1}^{K}$ are

$$\hat{\boldsymbol{a}}_j = \left(\hat{\boldsymbol{A}}^H\hat{\boldsymbol{A}}\right)^{-1}\hat{\boldsymbol{A}}^H\tilde{\boldsymbol{y}}_j, \quad j = 1, \cdots, J \quad (39)$$

When the signal-to-noise ratio (SNR) is low or when the data model is only approximately sound, the MODE frequency estimates may be so close to one another [13–15] that the amplitude estimates are very poor owing to the inversion of an ill-conditioned matrix $\hat{\boldsymbol{A}}^H\hat{\boldsymbol{A}}$. To circumvent this problem we modify MODE with the following frequency spacing adjustment scheme:

- Sort the MODE range frequency estimates $\{\hat{f}_k\}_{k=1}^{K}$ in an ascending order and then calculate the spacing between any two adjacent estimates.
- If the distance between two estimates, say $\Delta\hat{f}_k = \hat{f}_{k+1} - \hat{f}_k$, is less than a predefined threshold, say Δf_t, adjust the estimates by replacing $\hat{f}_k$ and $\hat{f}_{k+1}$ with $\hat{f}_k - 0.5\Delta f_t$ and $\hat{f}_{k+1} + 0.5\Delta f_t$, respectively. In our numerical examples, we choose $\Delta f_t = 1/(10N)$.

The amplitude estimates are then obtained by using the adjusted range frequency estimates with eqn. 39. (Although the spacing adjustment scheme is *ad hoc*, it turns out to be able to provide good initial estimates $\{\hat{\alpha}_k, \hat{f}_k\}_{k=1}^{K}$ for the last step of MRELAX). We refer to this approach of estimating $\{\{\alpha_{kj}\}_{j=1}^{J}, f_k\}_{k=1}^{K}$ as the modified MODE algorithm. Accordingly, the range feature extraction algorithm with MODE followed by the last step of MRELAX is referred to as MODE-MRELAX.

3.3 Estimation of scatterer number

We consider using the the generalised Akaike information criterion (GAIC) [20, 21] to determine the number of scatterers K. By assuming that the noise is white Gaussian, the estimate $\hat{K}$ of K can be determined as an integer that minimises the following GAIC cost function:

$$\begin{aligned}\text{GAIC}(\check{K}) &= NLJ \ln \sum_{j=1}^{J}\left\| \boldsymbol{y}_j - \hat{\bar{\boldsymbol{f}}}_r \odot \left[\hat{\psi} \otimes \left(\sum_{k=1}^{\check{K}} \hat{\alpha}_{kj}\hat{\boldsymbol{a}}_k\right)\right] - \boldsymbol{u}_L \otimes \hat{\boldsymbol{c}}_j \right\|^2 \\ &\quad + \delta \ln[\ln(NLJ)]\left[(2J+1)\check{K} + 2(L-1) + 2NJ + 1\right] \end{aligned} \quad (40)$$

where δ is a parameter of user choice, $[(2J+1)\check{K} + 2(L-1) + 2NJ + 1]$ denotes the total number of unknown real-valued parameters in the data model of eqn. 16, of which, $2J\check{K}$ is due to the complex amplitudes, $\check{K}$ to the range frequencies, $2(L-1)$ to the range migrations and phase errors, $2NJ$ to the clutter, and another 1 to the noise variance.

3.4 Initialisation

Observe that the stationary clutter can be cancelled out by subtracting $y_j(n, l)$ from $y_j(n, l+1)$. Note that we use this clutter cancellation scheme only for initialisation since this scheme will significantly weaken the signal power for slowly moving target and double the noise power. Let

$$\begin{aligned} x_j(n, l) &= y_j(n, l+1) - y_j(n, l) \\ &= \left(\sum_{k=1}^{K}\alpha_{kj}e^{j2\pi f_k n}\right)\left[e^{j(2\pi\bar{f}_{l+1}n + \psi_{l+1})} - e^{j(2\pi\bar{f}_l n + \psi_l)}\right] \\ &\quad + e_j(n, l+1) - e_j(n, l) \end{aligned}$$

$$n = 0, \ldots, N-1, \quad l = 0, \ldots L-2, \quad j = 1, \ldots J \quad (41)$$

Assume that the location change of a scatterer between two adjacent pulses is small with respect to the resolution size. Let $\bar{f}_{l+1} \simeq \bar{f}_l$ in eqn. 41, we have

$$x_j(n, l) \simeq \left(\sum_{k=1}^{K}\alpha_{kj}e^{j2\pi f_k n}\right)e^{j2\pi\bar{f}_l n}\rho_l + \tilde{e}_j(n, l)$$

$$n = 0, \ldots, N-1, \quad l = 0, \ldots, L-2, \quad j = 1, \ldots, J \quad (42)$$

where $\rho_l = e^{j\psi_{l+1}} - e^{j\psi_l}$ and $\tilde{e}_j(n, l) = e_j(n, l+1) - e_j(n, l)$. Let

$$\tilde{\rho}_l = \frac{\rho_l}{\rho_0} = \frac{e^{j\psi_{l+1}} - e^{j\psi_l}}{e^{j\psi_1} - 1}, \quad l = 1, \ldots, L-2 \quad (43)$$

Then the NLS estimates $\{\hat{\tilde{\rho}}_l, \hat{\bar{f}}_l\}_{l=1}^{L-2}$ of $\{\tilde{\rho}_l, \bar{f}_l\}_{l=1}^{L-2}$ can be obtained by minimising the following cost function:

$$C_8(\tilde{\rho}_l, \bar{f}_l) = \sum_{j=1}^{J}\|\boldsymbol{x}_{lj} - \tilde{\rho}_l(\boldsymbol{x}_{0j} \odot \bar{\boldsymbol{f}}_l)\|^2, \quad l = 1, \ldots, L-2 \quad (44)$$

where

$$\begin{aligned}\boldsymbol{x}_{lj} &= [x_j(0, l) \;\; x_j(1, l) \;\; \ldots \;\; x_j(N-1, l)]^T, \\ &\quad l = 0, 1, \ldots, L-2, \quad j = 1, \ldots, J \end{aligned} \quad (45)$$

The solutions that minimise C_8 in eqn. 44 are

$$\hat{\bar{f}}_l = \arg\max_{\bar{f}} |\bar{\boldsymbol{f}}_l^H\bar{\boldsymbol{x}}_l|, \quad l = 1, \ldots, L-2 \quad (46)$$

and

$$\hat{\tilde{\rho}}_l = \frac{\hat{\tilde{\boldsymbol{f}}}_l^H \bar{\boldsymbol{x}}_l}{\frac{1}{J}\sum_{j=1}^{J}(\boldsymbol{x}_{0j}^H \boldsymbol{x}_{0j})}, \quad l = 1, \ldots, L-2 \tag{47}$$

where

$$\bar{\boldsymbol{x}}_l = \frac{1}{J}\sum_{j=1}^{J}(\boldsymbol{x}_{0j}^* \odot \boldsymbol{x}_{lj}), \quad l = 1, \ldots, L-2 \tag{48}$$

The initial estimates $\{\hat{\psi}_l\}_{l=2}^{L-1}$ of $\{\psi_l\}_{l=2}^{L-1}$ can be obtained from $\{\hat{\tilde{\rho}}_l\}_{l=1}^{L-2}$ (eqn. 43)

$$\hat{\psi}_l = 2\ \text{angle}\left(\sum_{i=1}^{l-1}\hat{\tilde{\rho}}_i\right), \quad l = 2, \ldots, L-1 \tag{49}$$

Then the initial estimate $\hat{\psi}_1$ of ψ_1 can be computed easily from $\hat{\tilde{\rho}}_1$ and $\hat{\psi}_2$. Let

$$\tilde{x}_j(n,l) = \frac{e^{-j2\pi\hat{\tilde{f}}_l n}}{\hat{\rho}_l} x_j(n,l), \quad n = 0, \ldots, N-1,$$
$$l = 0, \ldots, L-2, \quad j = 1, \ldots, J \tag{50}$$

Then the initial estimates $\{\{\hat{\alpha}_{kj}\}_{j=1}^{J}, \hat{f}_k\}_{k=1}^{K}$ of $\{\{\alpha_{kj}\}_{j=1}^{J}, f_k\}_{k=1}^{K}$ can be obtained by applying MODE-MRELAX to $\tilde{x}_j(n,l)$. The clutter estimates $\{\hat{\boldsymbol{c}}_j\}_{j=1}^{J}$ can be initialised by

$$\hat{c}_j(n) = \frac{1}{L}\sum_{l=0}^{L-1}\left[y_j(n,l) - \left(\sum_{k=1}^{K}\hat{\alpha}_{kj}e^{j2\pi\hat{f}_k n}\right)e^{j2\pi\hat{\tilde{f}}_l n}e^{j\hat{\psi}_l}\right]$$
$$n = 0, \ldots, N-1, \quad j = 1, \ldots, J \tag{51}$$

where we have used $\hat{\tilde{f}}_{L-1} = \hat{\tilde{f}}_{L-2}$ as an initial estimate.

3.5 Summary of parameter estimation algorithm

The steps of polarimetric parameter estimation algorithm can be summarised as follows:

Step 0: Get the initial estimates of the moving target features and the initial clutter estimate according to Section 3.4.

Step 1: Update the range feature estimates $\{\{\hat{\alpha}_{kj}\}_{j=1}^{J}, \hat{f}_k\}_{k=1}^{K}$ with the last step of MRELAX by using the most recent estimates of $\{\tilde{f}_l, \psi_l\}_{l=1}^{L-1}$ and $\{\boldsymbol{c}_j\}_{j=1}^{J}$.

Step 2: Update the range migration and phase error estimates $\{\hat{\tilde{f}}_l, \hat{\psi}_l\}_{l=1}^{L-1}$, with eqns. 33 and 34, respectively, by using the most recently obtained $\{\{\hat{\alpha}_{kj}\}_{j=1}^{J}, \hat{f}_k\}_{k=1}^{K}$ and $\{\hat{\boldsymbol{c}}_j\}_{j=1}^{J}$.

Step 3: Update the clutter estimate $\{\hat{\boldsymbol{c}}_j\}_{j=1}^{J}$ with eqn. 28 by using the most recent $\{\{\hat{\alpha}_{kj}\}_{j=1}^{J}, \hat{f}_k\}_{k=1}^{K}$ and $\{\hat{\tilde{f}}_l, \hat{\psi}_l\}_{l=1}^{L-1}$.

Step 4: Iterate steps 1–3 until practical convergence is reached, i.e. when ϵ, the relative change of the cost function C_1 in eqn. 25 between two consecutive iterations, is less than 10^{-3}.

Step 5: Update $\{\{\hat{\alpha}_{kj}\}_{j=1}^{J}, \hat{f}_k\}_{k=1}^{K}$ by the modified MODE followed by the last step of MRELAX.

Step 6: Repeat steps 2, 3, and 5 several times.

Step 7: Iterate steps 2, 3, and 1 again until practical converge with $\epsilon \leq 10^{-6}$.

As for case 2, where the H- and V-polarised transmitted pulses are offset in time from one another by a half PRI, steps 0, 1, and 2 need some modification. In step 0, two sets of initial estimates are obtained from the first two channels ($J=2$) and the third channel ($J=1$), respectively. Since the range migration due to the first pulse in the third channel $\tilde{f}_{03} \neq 0$, we use $\tilde{f}_{03} = \hat{\tilde{f}}_{11}/2$ as an initial estimate of $\tilde{f}_{03}$. In step 1, when updating the range feature estimates, the motion compensation (eqn. 38) is separately performed in different channels by using the corresponding motion parameter estimates. In step 2, two sets of motion parameters are estimated from the first two channels and the third channel, respectively.

4 Numerical examples

Numerical examples illustrate the performance of the proposed algorithm for feature extraction with polarisation diversity. In the following examples the number of samples of the received signal associated with each pulse is $N=32$. We use $\epsilon \leq 10^{-3}$ to test the 'practical convergence' when performing steps 1 and 4 of the algorithm, and use $\epsilon \leq 10^{-6}$ when performing step 7. We use $\Delta f_t = 1/(10N)$ in the modified MODE algorithm as a minimum spacing threshold.

We assume that the target consists of only two closely spaced scatterers. The frequencies of the two scatterers are chosen as $f_1 = 0.2$ and $f_2 = f_1 + 1/4N$ in all examples. Both the clutter and noise are simulated as zero-mean white complex gaussian random processes. The signal-to-clutter ratio (SCR), defined as the ratio of a scatterer's intensity in the first polarisation channel to the clutter variance, is chosen as -20 dB in all the examples. The signal-to-noise ratio (SNR), defined as the ratio of the scatterer's intensity in the first polarisation channel to the noise variance, is chosen in an appropriate range in the examples where the pulse number is fixed, and as 20 dB when the pulse number varies. The phase errors are samples of a uniformly distributed variable within $[0, 2\pi)$, and the motion of the target is simulated as an accelerated motion with a small fluctuation in each pulse interval. Both the range migration and phase errors are fixed from trial to trial. In addition, for each polarisation channel, the clutter is independent for different polarisation channels but fixed from pulse to pulse and from trial to trial for each channel while the noise is independent for all pulses and trials. The parameter estimate performance is evaluated by comparing the mean-squared errors (MSEs), which are computed from 100 Monte Carlo trials, with the corresponding Cramér–Rao bounds (CRBs) under different SNRs and different pulse numbers.

First consider an example to illustrate the performance of the proposed feature extraction algorithm under different SNRs. The pulse number is fixed at $L=10$. The scattering matrices of two scatterers are chosen as

$$\boldsymbol{S}_1 = \begin{bmatrix} 1 & 0.2e^{j\pi/8} \\ 0.2e^{j\pi/8} & -\dfrac{1}{\sqrt{2}} \end{bmatrix}$$
$$\text{and} \quad \boldsymbol{S}_2 = \begin{bmatrix} 1 & 0.1e^{j\pi/4} \\ 0.1e^{j\pi/4} & \sqrt{2} \end{bmatrix} \tag{52}$$

These two scatterers can be interpreted, respectively, as an even-bounce scatterer, which is similar to a dihedral corner reflector, and an odd-bounce scatterer, which is similar to a trihedral corner reflector or a large conducting sphere.

In addition to the two full-polarisation cases mentioned in Section 2, a single HH channel is also considered in this sample, referred to as case 3, for comparison. In case 2 we assume the amplitude parameters $\{\alpha_{k3}\}_{k=1}^{K}$ to be real-valued for the third channel, and modify our algorithm in steps 0, 1, and 2 as described in Section 3.5. The GAIC with $\delta=3$ is used in this example to determine $\hat{K}$, the estimate of the number of scatterers, and $\hat{K}=2$ is obtained. The MSEs of the parameter estimates are compared with their corresponding CRBs as a function of SNR in Fig. 1.

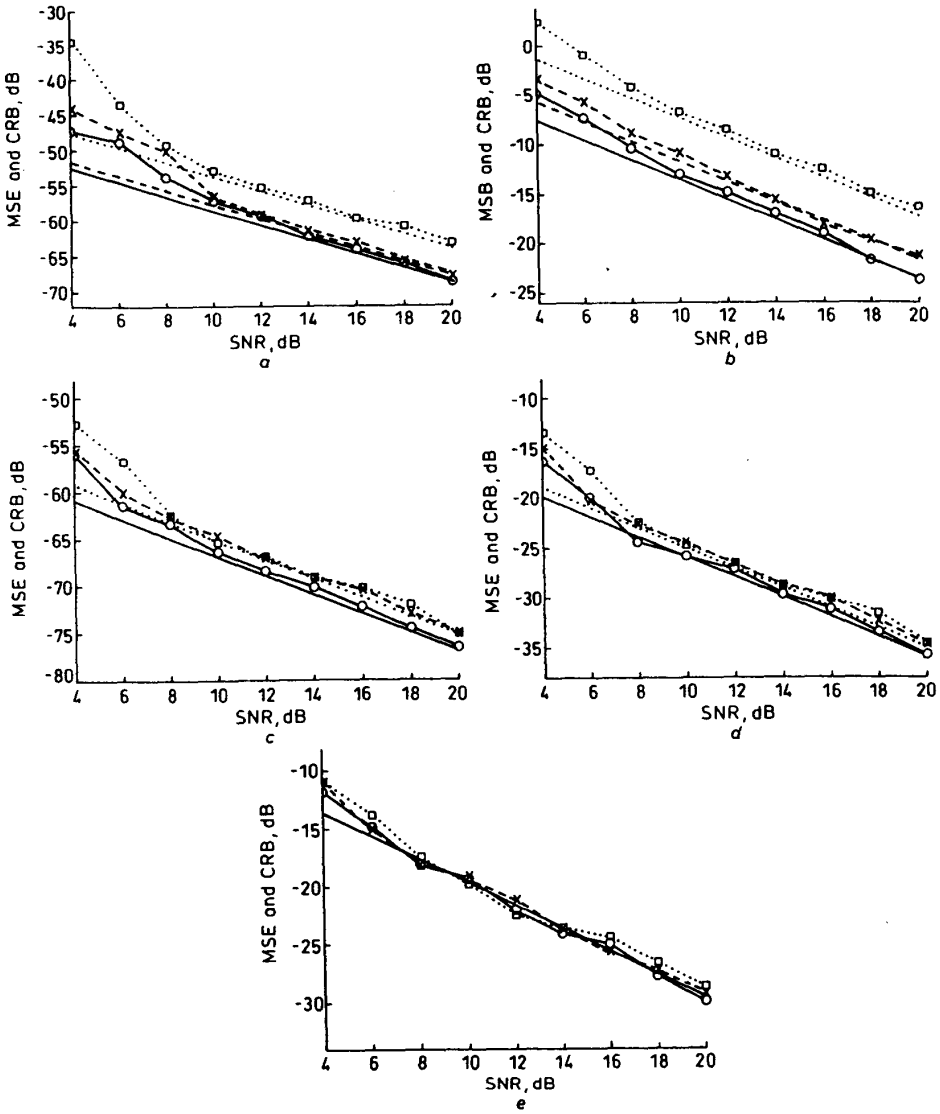

Fig. 1 *Comparison of MSEs with CRBs as a function of SNR $|f_2 - f_1| = 1/(4N)$, $N = 32$, $L = 10$, and SCR $= -20$ dB; first polarisation channel*

a Range of first scatterer
b RCS of first scatterer
c Range migration
d Phase error of second pulse
e First clutter sample
——— CRB (case 1)
—○— MSE (case 1)
– – – CRB (case 2)
– – × – – MSE (case 2)
····· CRB (case 3)
···□···MSE (case 3)

Fig. 1*a–e* are, respectively, for the frequency and amplitude of the first scatterer for the first polarisation channel, the range migration and phase error for the second pulse, and the first clutter sample for the first polarisation channel. The curves expressed by solid line and solid line with '○' are for case 1 for the CRBs and MSEs, respectively, the curves for case 2 are indicated by dotted-line and dotted-line with '×', and the dashed line and dashed line with '□' are for case 3. The CRBs for the estimates of range migration, phase error and clutter for case 2 are not shown in Figs. 1*c–e* to avoid too many lines in these Figures. Results in Figs. 1*a–e* show that the MSEs of the parameter estimates approach the corresponding CRBs as the SNR increases. Comparison between cases 1 and 2 with case 3 show that the feature extraction with polarisation diversity can remarkably outperform that without polarisation diversity. Compared with case 2, case 1 appears to be slightly better.

Next, we test the performance of the feature extraction algorithm under different pulse numbers. We fix the SNR at 20 dB, increase the pulse number from 6 to 14, and keep all other parameters the same as in the first example. Fig. 2 shows that the MSEs of parameter estimates obtained with the proposed algorithm can approach the corresponding

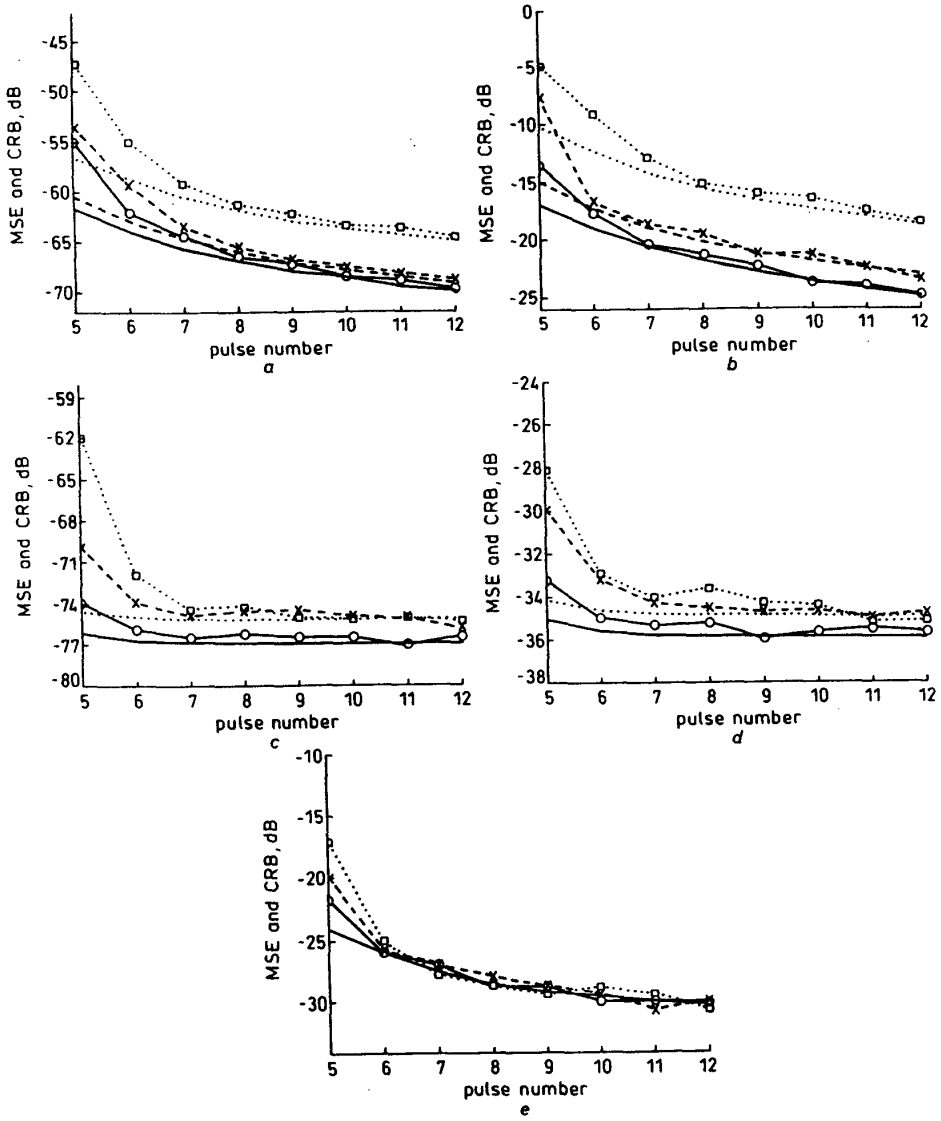

Fig. 2 *Comparison of MSEs with CRBs as a function of pulse number* $|f_2 - f_1| = 1/(4N)$, $N = 32$, $SNR = 20\,dB$, *and* $SCR = -20\,dB$; *first polarisation channel*

a Range
b RCS of the first scatterer
c Range migration
d Phase error of second pulse
e First clutter sample
——— CRB (case 1)
—○— MSE (case 1)
– – – – CRB (case 2)
– – × – – MSE (case 2)
····· CRB (case 3)
···□···MSE (case 3)

CRBs as the pulse number increases. Similar improvements in parameter estimates as a result of using polarisation diversity are observed in Fig. 2.

5 Conclusions

We have studied moving target feature extraction for the HRR MTI radar with polarisation diversity. A relaxation based algorithm has been presented for super resolution moving target feature extraction in a strong stationary clutter environment and in the presence of arbitrary range migration and arbitrary phase errors. Numerical results have shown that the proposed algorithm performs well, and that the MSEs of the parameter estimates can approach the corresponding CRBs as the SNR or pulse number increases. The advantages of moving target feature extraction with polarisation diversity over that without polarisation diversity have been demonstrated.

6 Acknowledgments

This work was supported in part by the Defense Advanced Research Project Agency contract ANTEON 98-1406-13-1 under the Mission Research Corporation subcontract

SC-1406-98-0004, the Office of Naval Research grant N00014-96-0817, and the National Science Foundation grant MIP-9457388. We acknowledge Mr. Z. Bi, Ms. N. Jiang, and Mr. J. Man for their many helpful discussions.

7 References

1 NOVAK, L.M.: 'A comparison of 1-D and 2-D algorithms for radar target classification'. Proceedings of the 1991 IEEE international conference on *Systems Engineering*, pp. 6–12, August 1991, Fairborn, OH, USA, pp. 6–12

2 MUSMAN, S., KERR, D., and BACHMANN, C.: 'Automatic recognition of ISAR ship images', *IEEE Trans. Aerosp. Electron. Syst.*, 1996, **32**, (4), pp. 1392–1404

3 FENNELL, M.T., and WISHNER, R.P.: 'Battlefield awareness via synergistic SAR and MTI exploitation', *IEEE Aerosp. Electron. Syst. Mag.*, 1998, **13**, (2), pp. 39–45

4 GOODMAN, R., NAGY, W., WILHELM, J., and CRIPPEN, S.: 'A high fidelity ground to air imaging radar system'. Proceedings of the 1994 IEEE National Conference on *Radar*, Atlanta, GA, pp. 29–34, March 1994

5 SCHLEHER, D.C.: 'MTI and pulsed doppler radar' (Artech House Norwood, MA, 1991)

6 WEHNER, D.R.: 'High resolution radar' (Artech House Norwood, MA, 1987)

7 BI, Z., WU, R., LI, J., and WILLIAMS, R.: 'Joint super resolution moving target feature extraction and stationary clutter suppression', *IEE Proc. - Radar, Sonar Navig.*, 2000, **147**, (1), pp. 23–29

8 ULABY, F.T., and ELACHI, C.: 'Radar polarimetry for geoscience applications' (Artech House Norwood, MA, 1990)

9 ZEBKER, H.A., and VAN ZYL, J.J.: 'Imaging radar polarimetry: A review', *Proc. IEEE*, 1991, **79**, pp. 1583–1606

10 NOVAK, L.M., BURL, M.C., and IRVINE, W.W.: 'Optimal polarimetric processing for enhanced target detection', *IEEE Trans. Aerosp. Electron. Syst.*, 1993, **29**, pp. 234–244

11 NOVAK, L.M., HALVERSEN, S.D., OWIRKA, G.J., and HIETT, M.: 'Effects of polarization and resolution on SAR ATR', *IEEE Trans. Aerosp. Electron. Syst.*, 1997, **33**, (1), pp. 102–116

12 LEE, J.S., GRUNES, M.R., AINSWORTH, T.L., DU, L.J., SCHULER, D.L., and CLOUDE, S.R.: 'Unsupervised classification using polarimetric decomposition and the complex Wishart classifier', *IEEE Trans. Geosci. Remote Sens.*, 1999, **37**, pp. 2249–2258

13 STOICA, P., and SHARMAN, K.C.: 'Novel eigenanalysis method for direction estimation', *IEE Proc. F*, 1990, **137**, pp. 19–26

14 STOICA, P., and SHARMAN, K.C.: 'Maximum likelihood methods for direction-of-arrival estimation', *IEEE Trans. Acoust. Speech Signal Process.*, 1990, **ASSP-38**, pp. 1132–1143

15 LI, J., STOICA, P., and LIU, Z.: 'Comparative study of IQML and MODE for direction-of-arrival estimation', *IEEE Trans. Signal Process.*, 1998, **46**, pp. 149–160

16 LI, J., ZHENG, D., and STOICA, P.: 'Angle and waveform estimation via RELAX', *IEEE Trans. Aerosp. Electron. Syst.*, 1997, **33**, pp. 1077–1087

17 TSANG, L., KONG, J.A., and SHIN, R.T.: 'Theory of microwave remote sensing' (Wiley, New York, 1985)

18 GOLUB, G.H., and VAN LOAN, C.F.: 'Matrix computations' (Johns Hopkins University Press, Baltimore, MD, 1984)

19 ZANGWILL, W.I.: 'Nonlinear programming: A unified approach' (Prentice-Hall, Englewood Cliffs, NJ, 1969)

20 SÖDERSTRÖM, T., and STOICA, P.: 'System identification' (Prentice-Hall, London, UK, 1989)

21 STOICA, P., EYKHOFF, D., JANSSEN, P., and SÖDERSTRÖM, T.: 'Model structure selection by cross-validation', *Int. J. Control*, 1986, **43**, (6), pp. 1841–1878

22 BANGS, W.: 'Array processing with generalized beamformers'. PhD dissertation, Yale University, New Haven, CT, 1971

23 STOICA, P., and MOSES, R.L.: 'Introduction to spectral analysis' (Prentice-Hall, Englewood Cliffs, NJ, 1997)

8 Appendix: Derivation of CRBs

The CRB matrix corresponding to the data model in eqn. 16 is derived for the case that the noise covariance matrix is arbitrary and unknown. The CRB matrices for the dual-polarisation and single-polarisation cases can be obtained similarly.

Let $\boldsymbol{Q}=E\{\boldsymbol{e}\boldsymbol{e}^H\}$, where $E\{\boldsymbol{X}\}$ denotes the expected value of $\boldsymbol{X}$. Then according to the extended Slepian–Bangs' formula, the ijth element of the Fisher information matrix (FIM) has the form [22, 23]

$$\{\mathrm{FIM}\}_{ij}=\mathrm{tr}\left(\boldsymbol{Q}^{-1}\boldsymbol{Q}_i'\boldsymbol{Q}^{-1}\boldsymbol{Q}_j'\right)+2\mathrm{Re}\left\{\left[(\boldsymbol{\Omega}\boldsymbol{a}+\boldsymbol{c})^H\right]_i'\boldsymbol{Q}^{-1}(\boldsymbol{\Omega}\boldsymbol{a}+\boldsymbol{c})_j'\right\} \quad (53)$$

where $\boldsymbol{\Omega}=\mathrm{diag}(\boldsymbol{u}_J)\times[(\bar{\boldsymbol{f}}\boldsymbol{u}_k^T)\odot(\boldsymbol{\psi}\times\boldsymbol{A})]$, $\boldsymbol{a}=[\boldsymbol{a}_1^T\ldots\boldsymbol{a}_J^T]^T\in C^{KJ\times 1}$, $\boldsymbol{c}=[\boldsymbol{c}_1^T\ldots\boldsymbol{c}_J^T]^T$, $\boldsymbol{u}_J\in R^{J\times 1}$ and $\boldsymbol{u}_K\in R^{K\times 1}$ have the same form as $\boldsymbol{u}_L$ in eqn. 17, $\boldsymbol{X}_i'$ denotes the derivative of $\boldsymbol{X}$ with respect to the ith unknown parameter, and $\mathrm{tr}(\boldsymbol{X})$ denotes the trace of $\boldsymbol{X}$. Note that the FIM is block diagonal since the parameters in $\boldsymbol{Q}$ are independent of those in $(\boldsymbol{\Omega}\boldsymbol{a}+\boldsymbol{c})$ and *vice versa*. Hence, the CRB matrix for the target features and the motion parameters can be calculated from the second term on the right side of eqn. 53. Let

$$\boldsymbol{\eta}=\left[\mathrm{Re}^T(\boldsymbol{a})\quad \mathrm{Im}^T(\boldsymbol{a})\quad \boldsymbol{f}^T\quad \boldsymbol{f}_r^T\quad \boldsymbol{\psi}_r^T\quad \mathrm{Re}^T(\boldsymbol{c})\quad \mathrm{Im}^T(\boldsymbol{c})\right] \quad (54)$$

where $\boldsymbol{f}=[f_1\cdots f_K]^T$, $\boldsymbol{f}_r=[\bar{f}_0\cdots\bar{f}_{L-1}]^T$, and $\boldsymbol{\psi}_r=[\psi_0\cdots\psi_{L-1}]^T$. Let

$$\boldsymbol{F}_1=\boldsymbol{\Omega} \quad (55)$$

$$\boldsymbol{F}_2=j\boldsymbol{F}_1 \quad (56)$$

$$\boldsymbol{F}_3=\left[(\boldsymbol{\Omega}_1\mathrm{diag}(\boldsymbol{a}_1))^T\quad\cdots\quad(\boldsymbol{\Omega}_1\mathrm{diag}(\boldsymbol{a}_J))^T\right]^T \quad (57)$$

where $\boldsymbol{\Omega}_1=j2\pi(\bar{\boldsymbol{f}}\boldsymbol{u}_K^T)\odot\boldsymbol{\psi}\otimes[(\boldsymbol{d}_N\boldsymbol{u}_K^T)\odot\boldsymbol{A}]$, with $\boldsymbol{d}_N=[0\ 1\cdots N-1]^T\in R^{N\times 1}$,

$$\boldsymbol{F}_4=\left[\boldsymbol{\Phi}_1^T\quad\boldsymbol{\Phi}_2^T\quad\cdots\quad\boldsymbol{\Phi}_J^T\right]^T \quad (58)$$

where $\boldsymbol{\Phi}_1=j2\pi(\bar{\boldsymbol{f}}\boldsymbol{u}_K^T)\odot\{\boldsymbol{\psi}\otimes[(\boldsymbol{d}_N\odot(\boldsymbol{A}\boldsymbol{a}_j))\boldsymbol{u}_L^T]\}\odot[\boldsymbol{I}_L\otimes\boldsymbol{u}_N]$, $j=1,\ldots,J$, with $\boldsymbol{I}_L$ being the $L\times L$ identity matrix,

$$\boldsymbol{F}_5=\left[\boldsymbol{\Psi}_1^T\quad\boldsymbol{\Psi}_2^T\quad\cdots\quad\boldsymbol{\Psi}_J^T\right]^T \quad (59)$$

where $\boldsymbol{\Psi}_j=j(\bar{\boldsymbol{f}}\boldsymbol{u}_K^T)\odot\{\boldsymbol{\psi}\otimes[(\boldsymbol{A}\boldsymbol{a}_j)\boldsymbol{u}_L^T]\}\odot[\boldsymbol{I}_L\otimes\boldsymbol{u}_N]$, $j=1,\ldots,J$. Let

$$\boldsymbol{F}_6=\boldsymbol{I}_J\otimes(\boldsymbol{u}_L\otimes\boldsymbol{I}_N) \quad (60)$$

and

$$\boldsymbol{F}_7=j\boldsymbol{F}_6 \quad (61)$$

Then let

$$\boldsymbol{F}=\left[\boldsymbol{F}_1\quad\boldsymbol{F}_2\quad\boldsymbol{F}_3\quad\boldsymbol{F}_4\quad\boldsymbol{F}_5\quad\boldsymbol{F}_6\quad\boldsymbol{F}_7\right] \quad (62)$$

The CRB matrix for the parameter vector $\boldsymbol{\eta}$ is given by

$$\mathrm{CRB}(\boldsymbol{\eta})=[2\mathrm{Re}(\boldsymbol{F}^H\boldsymbol{Q}^{-1}\boldsymbol{F})]^{-1} \quad (63)$$

Note that the CRB matrix given in eqn. 63 is independent of the clutter parameter $\{\boldsymbol{c}_j\}_{j=1}^J$ since all of the elements in $\boldsymbol{F}$ do not depend on $\{\boldsymbol{c}\}_{j=1}^J$.